

Variational Photocarrier Radiometry Reconstruction of Exciton Lifetime Spectra for a Coupled PbS Colloidal Quantum Dot Thin Film Under Combined AC and DC Laser Excitation

Jing Wang^{1,2} · Andreas Mandelis^{1,2} ·
Alexander Melnikov²

Received: 10 December 2013 / Accepted: 13 March 2015 / Published online: 24 March 2015
© Springer Science+Business Media New York 2015

Abstract Colloidal quantum dots (CQDs) have attracted significant interest for applications in electronic and optoelectronic devices such as photodetectors, light emitting diodes, and solar cells. However, a poor understanding of charge transport in these nanocrystalline films hinders their practical applications. The photocarrier radiometry (PCR) technique, a frequency-domain photoluminescence method spectrally gated for radiative recombination photon emissions and exclusion of thermal infrared photons, has been applied to a coupled PbS CQD thin film with inter-dot spacing of 0.5 nm to 1 nm for the analysis of charge transport properties. As the nanoparticle bandgap depends on the size of the quantum dots, polydispersity of the CQD thin film causes bandgap variability leading to photoexcited carrier (exciton) decay lifetime broadening and temperature dependence. The carrier transport mechanisms of QDs are quite different from bulk semiconductors, so the conventional carrier-diffusion wave-based PCR theory was modified into a non-diffusive limit model. A developed variational discrete lifetime reconstruction approach was used to analyze PCR frequency scans under two optical excitation modes: a modulated laser source without, and with, an additional continuous laser source. Using this model, the CQD mean lifetime values were found and variational discrete lifetime spectra were reconstructed.

Keywords Excitonic lifetime · Frequency domain · Lead sulfide · Nanoparticles · Precision measurements

✉ Andreas Mandelis
mandelis@mie.utoronto.ca

¹ School of Optoelectronic Information, University of Electronic Science and Technology of China, Chengdu 610054, Sichuan, China

² Center for Advanced Diffusion-Wave Technologies (CADIFT), Department of Mechanical and Industrial Engineering, University of Toronto, Toronto M5S 3G8, Canada

1 Introduction

Lead-salt colloidal quantum dots (CQDs) have been successfully employed as active components in electronic and optoelectronic devices such as photodetectors [1,2], light emitting diodes [3,4], and solar cells [5,6]. By adjusting the composition, size, shape, monodispersity, capping ligand, and surface chemistry, as well as the degree of superlattice order in the films, electronic and optical properties become tunable. Studies of lead-salt QDs have been carried out for several decades and still attract a growing number of investigations from both fundamental and applied points of view. However, as a commonly used tool for investigating QD photo-physics, DC photoluminescence (PL) to-date has not been accurate enough to determine the distribution of lifetimes. The development of reliable physical models of QD excited-state interactions as a function of parameters such as ambient temperature, QD, and trap densities can only be accomplished if the foregoing limitations on lifetime accuracy and precision/resolution can be overcome.

Photocarrier radiometry (PCR) [7–9], as a dynamic spectrally integrated frequency-domain PL modality, can yield quantitative information about relaxation lifetime distributions, and their radiative and non-radiative components associated with intra-QD and inter-QD excited-state decay processes with accuracy and precision superior to time-resolved PL due to its intrinsically high signal-to-noise ratio (SNR) based on narrowband lock-in demodulation. Coupled with a physical relaxation model, PCR can allow the formulation of an inverse problem approach to reconstructing lifetime distributions (spectra) as a function of temperature, thereby probing various intra- and inter-QD relaxation processes. This process can successfully link definitive physical models to the decay rates of exciton relaxation mechanisms.

In this work, to give insight into the potential physical origins of the associated exciton relaxation mechanisms and inter-QD exciton transport processes involved in coupled PbS CQD thin films, a developed variational discrete lifetime reconstruction approach was used to analyze PCR frequency scans under two optical excitation modes: a modulated laser source without, and with, an additional continuous laser source.

2 Lifetime Calculation Methodology

Clark et al. [10] observed in a close-packed PbS QD solution that different fluorescence wavelengths are characterized by different decay times which, in turn, are associated with Förster resonant energy transfer (FRET) between QDs of smaller and larger sizes, given the excitonic quantum energy level dependence on quantum dot size. They concluded that different wavelengths are emitted by quantum dots of continuous size distributions and different lifetimes. In general, a continuous distribution of sizes is expected in any QD sample, albeit narrow or wide even within a nominally single size quantum dot assembly. It is also reasonable to assume a correspondence between size and decay lifetime upon energy exchange between smaller dots (higher exciton energy levels) and larger dots (lower energy levels) [10,11].

In an earlier report [12], a continuous and two discrete lifetime distribution approaches were developed. The Gaussian distribution with a Voigt profile was found to be effective in describing exciton decay properties in an uncoupled QD sample, while the variational model was found appropriate for de-excitation mechanism analysis in a coupled assembly.

A time-domain approach to photoluminescence decay kinetics from carriers trapped in exciton states can be represented as

$$I(t) = \int_{\tau_{\min}}^{\tau_{\max}} f(\tau)e^{-t/\tau} d\tau. \quad (1)$$

The PCR frequency response of a PbS colloidal QDs system can be obtained from the Fourier transform:

$$F(\omega) = \int_0^{\infty} I(t)e^{-i\omega t} dt \simeq \int_0^{\infty} dt \int_{-\infty}^{\infty} f(\tau)e^{-t/\tau - i\omega t} d\tau, \quad (2)$$

where a continuous or discrete, but physically finite, distribution of lifetimes allows the truncated lower and upper limits of the lifetime integral (Eq. 2) to be approximated by the full range of possible lifetimes. Then the PCR frequency response of a PbS colloidal QD system can be obtained from the following integral of the relaxation lifetime distribution [12]:

$$F(\omega) = \int_0^{\infty} \frac{\tau f(\tau) d\tau}{1 + i\omega\tau}. \quad (3)$$

Equation 1 can be considered as an integral equation, where $f(\tau)$ is the (unknown) lifetime distribution function and $F(\omega)$ is a known function, a frequency response which can be measured experimentally. $f(\tau)$ can be extracted using inversion methods for integral equations. Here, only positive lifetimes have been considered. When resolved into its real and imaginary parts, Eq. 1 can be written in the form,

$$\int_0^{\infty} K_{R/I}(\omega\tau)\Psi_{R/I}(\tau)d\tau = F_{R/I}(\omega); \quad 0 \leq \omega < \infty \quad (4)$$

with the symmetric kernel,

$$K_R(\omega\tau) = \frac{1}{1 + (\omega\tau)^2}, \quad (5)$$

$$K_I(\omega\tau) = -\frac{\omega\tau}{1 + (\omega\tau)^2}, \quad (6)$$

and $\Psi_{R/I}(\tau)$ is the variational solution which represents the lifetime distribution function.

The PCR phase is known to be more sensitive than the amplitude to the details of relaxation times associated with luminescent (radiative) emission processes in opto-electronic systems [8,9], so here only solutions for the imaginary part are reproduced and the following discussion is mainly based on the results from phase (or quadrature) fitting.

When assuming the existence of multiple (n) discrete time constants τ_i in a dynamic system, the variational solution for the imaginary part is

$$\Psi_1(\tau) = \sum_{i=1}^n \beta_i \tau \delta(\tau - \tau_i) \equiv \sum_{i=1}^n \beta_i \Psi_{1i}(\tau). \quad (7)$$

Thus, the calculated β_i coefficients can be used to build the discrete lifetime spectrum from the imaginary parts of the frequency data (lock-in quadrature signal). The two spectra from real and imaginary parts are theoretically identical; however, in practice, there are differences by virtue of the nature of the two lock-in data channels. A mean decay lifetime can be calculated as

$$\bar{\tau} = \left(\sum_{i=1}^n \beta_i \tau_i^2 \right) / \left(\sum_{i=1}^n \beta_i \tau_i \right). \quad (8)$$

3 Experimental Materials and System

A coupled PbS QD sample with a quantum dot mean diameter of 4.2 nm and inter-particle spacing of about 0.5 nm to 1 nm was studied [13]. Such spacings allow for strong interactions between dots resulting in a coupled QD system. A schematic diagram of the PCR experimental setup was similar to our previous publications [9,12], as shown in Fig. 1. A 10 mW diode laser of 830 nm wavelength and a beam diameter of *ca.* 0.1 mm was square-wave modulated with a function generator. A 1 μ m long-pass filter was placed in front of the InGaAs photodetector to block the excitation beam. No short-pass filter was necessary as thermal infrared contributions to the signal were found to be negligible. The sample was placed on a Linkam LTS350 cryogenic stage, which allows maintaining a constant temperature in the 77 K to 520 K range. Here, another identical 830 nm diode laser was used as a DC excitation source.

4 Results and Discussion

Figure 2 shows the frequency-scanned PCR amplitude and phase responses. A decreasing temperature leads to pronounced growth of the PCR amplitude because of a decreased non-radiative recombination probability at lower temperatures which scales with the phonon population. The increasing high-frequency PCR phase lag with decreasing temperature is consistent with increased de-excitation lifetimes. A Gaussian lifetime distribution assumption $f(\tau) = f_0 e^{-[(\tau-\tau_0)/\Delta\tau]^2}$ could not yield good fits to the PCR signals; therefore, a Voigt profile is not appropriate to approximate

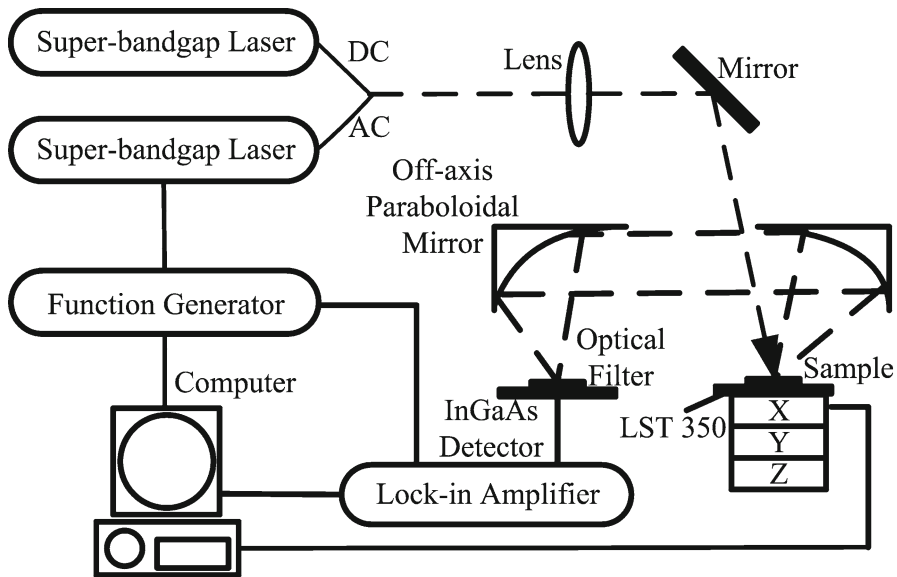


Fig. 1 Experimental setup of the photocarrier radiometry (PCR) system for CQD frequency and temperature scans

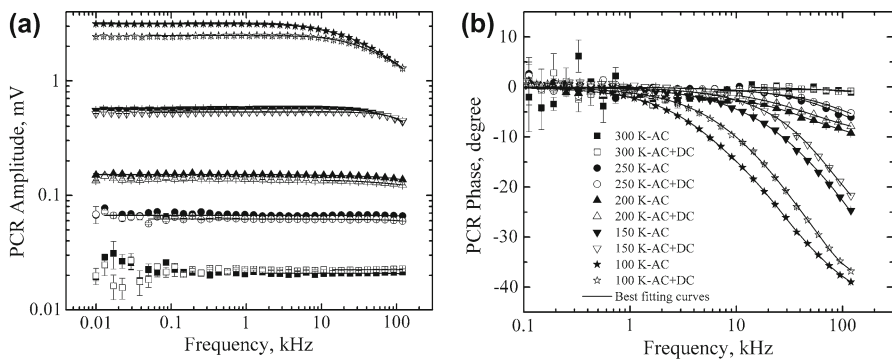


Fig. 2 PCR frequency scan spectra for a coupled PbS QD sample under AC laser illumination and AC+DC laser illumination. Best fitted curves were calculated from Eq. 4: (a) experimental amplitudes and (b) phases. Error bars, when not apparent, are of the size of, or smaller than, the symbols

the very complicated exciton de-excitation mechanism(s) for a coupled QD case due to the strong interactions among nearest, and possibly more remote, neighbors. The variational inverse lifetime distribution model [12] was used to fit real and imaginary channels of the PCR signals. The best-fit results were recast into amplitude and phase channels, as shown in Fig. 2.

$$S(\omega) = \sqrt{F_R^2(\omega) + F_I^2(\omega)} \quad (9)$$

$$\phi(\omega) = \tan^{-1} \left[\frac{F_I(\omega)}{F_R(\omega)} \right] \quad (10)$$

Equation 7 and its corresponding real part were used to reconstruct discrete lifetime spectra which are shown in Fig. 3a, b. Line spectra with weighting function values $\Psi_{1/R}(\tau) < 10\%$ of Ψ_{\max} were neglected.

The mean lifetime values are derived as 0.19 μs , 0.79 μs , 1.13 μs , 1.83 μs , and 6.58 μs between 100 K and 300 K, increasing with decreasing temperature. However, a degree of non-monotonicity is observed as a result of the appearance of additional major lifetime components at low temperatures (≤ 200 K) in the variational spectrum, and the dominant lifetime (the highest peak in each distribution) is strongly influenced by those additional peaks. Here, the variational peaks measure the most probable lifetime values.

For a thin film with a dense QD network, it is known that energy transfer from resonant energy states of smaller dots to higher excited states of larger dots in PbS dispersions is very efficient [10] and many nearest-neighbor-hopping (NNH) transitions occur at higher temperatures [14]. The inability to find a good Gaussian fit is indicative of the multiple de-excitation channel mechanisms associated with simultaneous and independent energy decay pathways. Additional relaxation degrees of freedom in these coupled lifetime distribution profiles are likely to involve nearest-neighbor inter-QD interactions in the form of excited-state electron tunneling (NNH migration or a Förster resonance) and photon emission from another QD, with the main difference being a more complicated inter-system crossing network for the coupled sample and therefore wider lifetime line spectrum. These pathways manifest themselves as additional lifetime peaks at $T \leq 200$ K, Fig. 3b. The quite strong increase of the radiative emission probability as represented by the variational coefficients β_i in Fig. 3b is also consistent with the short-range exciton–exciton interaction and the high probability of a hopping or tunneling exciton to enter the excited-state manifold of a neighboring quantum dot and decay or continue on to a tertiary excitonic site.

With the additional DC laser source, PCR frequency scans were also carried out, as shown in Fig. 2, labeled with corresponding temperatures and ‘AC+DC.’ The exciton mean lifetime values were found to be 0.56 μs , 0.93 μs , 1.02 μs , 1.17 μs , and 3.87 μs between 100 K and 300 K by fitting the quadrature signals with Eq. 4. The reconstructed lifetime distribution spectra are shown in Fig. 3c, d. Figure 2 shows that at most temperature points, with the additional DC laser, the exciton lifetime decreased (smaller phase lag), and the PCR amplitude also decreased. With the DC background, more exciton-excited states are occupied continuously upon photon absorption and, as such, the excitonic density increases even without AC illumination. When the AC light is turned on, then the formed excitons (same number as without DC light because the AC light intensity, or photon flux, does not change between the two situations) which would tunnel (“hop”) to otherwise unoccupied neighboring states cannot reach the available states but undergo repulsive exciton–exciton interactions (collisions) in a crowded exciton neighborhood in colloidal QDs. The result of the collisions is a shorter effective lifetime and a lower mean number density of active excitons. Furthermore, it is also interesting to note that the most reliable (imaginary signal deduced) lifetimes above 200 K are longer with the DC background than without. This could be due to more efficient exciton–exciton repulsive interactions in the presence of the excess excitons of the DC optical field and thus increased intra-exciton confinement leading to radiative relaxation rather than exciton–phonon scattering.

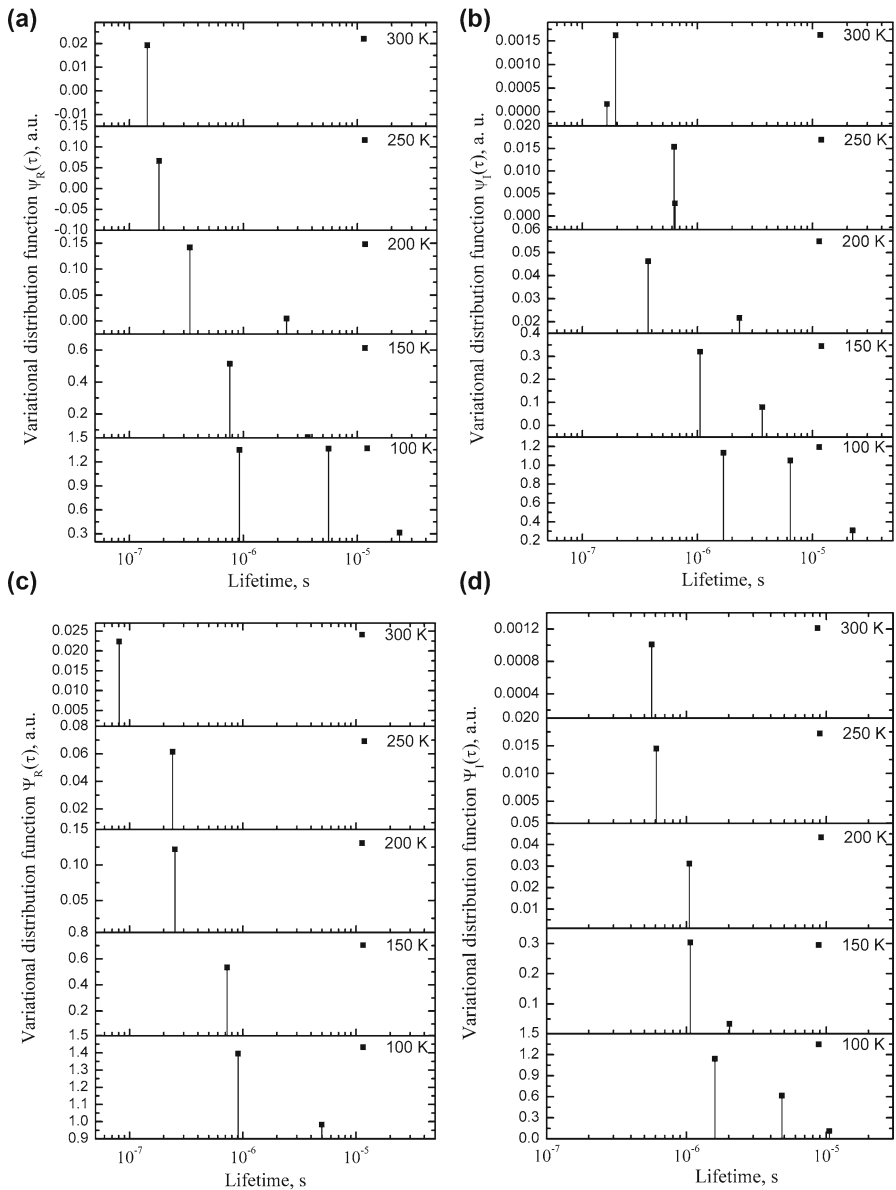


Fig. 3 Discrete exciton lifetime distribution spectra of the coupled sample at various temperatures reconstructed from PCR frequency scan lock-in data: (a) variational discrete lifetime distribution from the in-phase signal under AC laser illumination, (b) variational discrete lifetime distribution from the quadrature signal under AC laser illumination, (c) variational discrete lifetime distribution from the in-phase signal under AC+DC laser illumination, and (d) variational discrete lifetime distribution from the quadrature signal under AC+DC laser illumination

5 Conclusions

The PCR method was applied to the study of optoelectronic properties of PbS CQDs. Using a rigorous variational lifetime distribution model, lifetime distribution spectra were reconstructed from the PCR frequency-response data with a modulated laser source without and with additional optical DC excitation. The high lock-in signal-to-noise ratio inherent in PCR allowed the generation of reliable discrete lifetime spectra and yielded plausible physical mechanisms of intra-dot and inter-dot excitonic interactions. The highly reliable variational lifetime line spectrum can be further used to identify the temperature threshold for the onset of NNH and exciton–exciton hopping interactions in coupled CQD systems.

Acknowledgments A. Mandelis is grateful to the Natural Sciences and Engineering Research Council (NSERC) for a Discovery grant, to the Canada Foundation for Innovation (CFI) for equipment grants, and to the Canada Research Chairs Program, and to the Ontario Ministry for Research and Innovation (MRI) for the Inaugural Premier’s Discovery Award in Science and Technology (2007). J. Wang is grateful to the China Scholarship Council (CSC) for an international student grant, to the National Natural Science Foundation of China (Grant No. 61379013), and to the Central-University Basic Research Funds of UESTC (Grant No. ZYGX2012Z006).

References

1. J.P. Clifford, G. Konstantatos, K.W. Johnston, S. Hoogland, L. Levina, E.H. Sargent, *Nat. Nanotechnol.* **4**, 40 (2009)
2. G. Konstantatos, I. Howard, A. Fischer, S. Hoogland, J.P. Clifford, E. Klem, L. Levina, E.H. Sargent, *Nature* **442**, 180 (2006)
3. S. Coe, W.K. Woo, M. Bawendi, V. Bulovic, *Nature* **420**, 800 (2002)
4. A.H. Mueller, M.A. Petruska, M. Achermann, D.J. Werder, E.A. Akhador, D.D. Koleske, M.A. Hoffbauer, V.I. Klimov, *Nano Lett.* **5**, 1039 (2005)
5. K.W. Johnston, A.G. Pattantyus-Abraham, J.P. Clifford, S.H. Myrskog, D.D. MacNeil, L. Levina, E.H. Sargent, *Appl. Phys. Lett.* **92**, 151115 (2008)
6. S.A. McDonald, G. Konstantatos, S. Zhang, P.W. Cyr, E.J.D. Klem, L. Levina, E.H. Sargent, *Nat. Mater.* **4**, 138 (2005)
7. J. Batista, A. Mandelis, D. Shaughnessy, *Appl. Phys. Lett.* **82**, 4077 (2003)
8. J. Xia, A. Mandelis, *Appl. Phys. Lett.* **96**, 262112 (2010)
9. J. Xia, A. Mandelis, *J. Appl. Phys.* **105**, 103712 (2009)
10. S.W. Clark, J.M. Harbold, F.W. Wise, *J. Phys. Chem. C* **111**, 7302 (2007)
11. J.J. Peterson, T.D. Krause, *Nano Lett.* **6**, 510 (2006)
12. J. Wang, A. Mandelis, A. Melnikov, S. Hoogland, E.H. Sargent, *J. Phys. Chem. C* **117**, 23333 (2013)
13. A.G. Pattantyus-Abraham, I.J. Kramer, A.R. Barkhouse, X. Wang, G. Konstantatos, R. Debnath, L. Levina, I. Raabe, M.K. Nazeeruddin, M. Grätzel, E.H. Sargent, *ACS Nano* **4**, 3374 (2010)
14. J.H. Warner, E. Thomsen, A.R. Watt, N.R. Heckenberg, H. Rubinsztein-Dunlop, *Nanotechnology* **16**, 175 (2005)